A TECHNIQUE FOR DESIGNING EARTH–MARS LOW-THRUST TRANSFERS CULMINATING IN BALLISTIC CAPTURE

G. Aguiar

Delft University of Technology
Astrodynamics & Space Missions
Kluyverweg 1, 2629, Delft, The Netherlands

F. Topputo

Politecnico di Milano
Dept. of Aerospace Science and Technology
Via La Masa 34, 20156, Milano, Italy

ABSTRACT

It is possible to design heliocentric transfers to Mars culminating in ballistic capture. With an impulsive-thrust strategy, these have already been studied, but were found to be less fuel-efficient and longer-lasting than Hohmann transfers. The objective of the present work is to investigate the characteristics of Earth–Mars *low-thrust* transfers to ballistic capture.

Small spacecraft are very mass- and power-constrained, so orbit transfers are challenging for them, especially to interplanetary destinations. To try and shift this paradigm, the study was carried out assuming the spacecraft to be a 16-unit CubeSat. In addition, to improve the validity of the results, ballistic capture was designed using a model that included many perturbing forces, namely third-body perturbations, solar radiation pressure and non-spherical gravity.

Some capture orbits were selected, each with a different arrival date at Mars, and targeted from Earth, on multiple departure dates. It was found that if the spacecraft is given enough time, the low-thrust strategy requires roughly the same fuel regardless of Earth departure or Mars arrival dates. In addition, terminating a low-thrust transfer to Mars in ballistic capture *does not* carry additional costs, when compared to simply rendezvousing with the planet. With the assumed spacecraft and departure conditions, only around 5 kg of propellant are required to reach Mars and get ballistically captured. Nevertheless, the spacecraft needs to fly for at least 3.5 years, which can be challenging for a CubeSat.

Index Terms— Ballistic capture, Low-thrust transfer, Earth–Mars transfer, CubeSat, Perturbing forces

1. INTRODUCTION

The phenomenon by which a spacecraft can both approach a celestial body and start revolving around it, without needing to manoeuvre in between, is known as *ballistic capture* or gravitational capture [1, p. 31]. For ballistic capture to take place, the spacecraft must be under the gravitational influence of at least two celestial bodies [2]. However, if a spacecraft can be captured solely due to the gravitational attraction of celestial bodies, it can also inadvertently escape by means of the same mechanism. Therefore, the capture is temporary and, unless mechanical energy dissipation takes place, the spacecraft escapes or crashes after performing a certain number of revolutions.

Ballistic capture could prove especially useful for spacecraft with limited propulsion capabilities. This is the case of miniaturized satellites, like the ones following the *CubeSat* format. Small spacecraft are very mass-, volume- and power-constrained, so orbit transfers are challenging for them, especially to interplanetary destinations. This is, in part, due to the significant change in velocity traditionally required for *orbit insertion*. [3]

In [4], ballistic *capture sets* were manipulated with the sole purpose of finding transfers to Mars. This method is more systematic than simply targeting the Weak Stability Boundary (WSB) and, as shown in [2], can be generalized to consider a *real-Solar-System* model. Nevertheless, the transfers found can be *less* fuel-efficient and last *longer* than some Hohmann transfers.

The extra fuel spent by the transfers of [4] could be attributed to the fact that manoeuvres were simultaneously modelled as instantaneous changes in velocity (Δv) and performed at a considerably large distance from Mars, not taking advantage of what is known as the *Oberth* effect. This refers to the fact that a given Δv adds *more* kinetic energy to the spacecraft if it is applied at pericentre (and along the spacecraft's velocity vector).

Therefore, when searching for the benefits of having the spacecraft be gravitationally captured far away from Mars, applying instantaneous changes in velocity is not the best approach. However, those could be replaced by a slow velocity change up until the capture point. To put it in another way, chemical propulsion could be replaced by *continuous low-thrust* propulsion. While the present work was being written, [5] made this very same recommendation.

The different nature of the low-thrust strategy, together with the work of [4], inspired the present work, which aims to answer the following question:

What are the characteristics of Earth–Mars transfers that combine ballistic capture orbits and low-thrust propulsion?

The present document is organised as follows. Section 2 overviews the proposed concept of Earth–Mars transfer and Section 3 lists the assumptions made about the spacecraft. Then, Section 4 deals with the generation and selection of ballistic capture orbits, while Section 5 faces the design of transfers to those orbits. The main results are given in Section 6 and some final considerations are stated in Section 7.

The values of the physical constants used in the present work are listed in Table 1. Ephemerides of celestial bodies and International Astronomical Union (IAU) rotation models were retrieved using the SPICE system, publicly available in the "SPICE Toolkit" page of the Navigation and Ancillary Information Facility (NAIF) website. In particular, the data was retrieved from *kernels* `de430.bsp`, `mar097.bsp` and `pck00010.tpc`, publicly available in the "Generic Kernels" area of the NAIF server. The coefficients used to describe the mass distribution of Mars were retrieved from the MRO120D gravity field model, publicly available in the file `jgmro_120d_sha.tab`, archived in the Geosciences Node of the Planetary Data System (PDS).

Table 1. Physical constants used in this work. All listed bodies, except for Mars and the Sun, refer to a satellite system barycentre, when applicable. The index "Ph" stands for Phobos; "D" stands for Deimos.

Symbol	Value
L_{S}	$3.8458 \cdot 10^{26}$ W
c	299792.458 km/s
R_{M}	3396 km
R_{Ph}	13 km
R_{D}	7.8 km
$R_{\mathrm{SOI_M}}$	$577.13 \cdot 10^3$ km
g_0	9.80665 m/s^2

Body	GM (km^3/s^2)
Sun	$1.327124400419393 \cdot 10^{11}$
Mercury	$2.203178000000002 \cdot 10^4$
Venus	$3.248585920000000 \cdot 10^5$
Earth	$4.035032355022598 \cdot 10^5$
Mars	$4.282837581575610 \cdot 10^4$
Jupiter	$1.267127648000002 \cdot 10^8$
Saturn	$3.794058520000000 \cdot 10^7$
Uranus	$5.794548600000008 \cdot 10^6$
Neptune	$6.836527100580023 \cdot 10^6$

2. CONCEPT

The proposed concept of Earth–Mars transfer is defined by the following sequence of events (see Figure 1):

1. **Departure from Earth.** At time t_d, the spacecraft is assumed to depart: a) from the position of the Earth, displaced in the direction opposite to the Sun by $R_{\mathrm{SOI_E}}$, the radius of Earth's Sphere of Influence (SOI) with respect to the Sun; b) with the velocity of the Earth, with respect to the Sun.

2. **Powered flight.** The spacecraft can use its low-thrust engine to spiral out towards Mars, switching it on and off when appropriate.

3. **Beginning of ballistic capture.** At time t_f, the spacecraft achieves the state required for ballistic capture at Mars. So, from that point forward, the engine no longer needs to be used (neglecting trajectory correction manoeuvres). This event takes place outside Mars' SOI with respect to the Sun.

4. **Ballistic flight.** The spacecraft approaches Mars in a ballistic flight, during which it enters Mars SOI.

5. **Arrival at Mars.** At time t_0, the spacecraft makes its first closest approach to Mars.

6. **Revolutions.** The spacecraft completes a predefined number of revolutions around Mars.

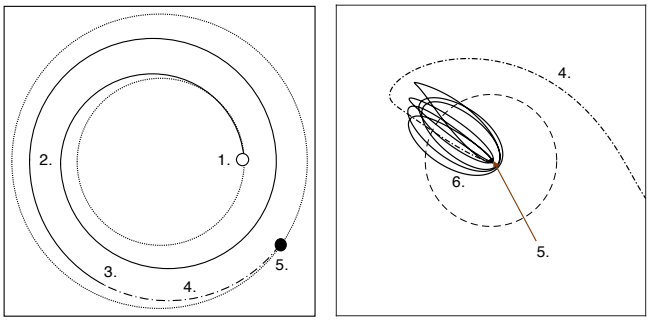

(a) Heliocentric view. (b) Areocentric view.

Fig. 1. Proposed concept of Earth-Mars transfer, combining low-thrust propulsion and ballistic capture. The numbers refer to the events or phases described in Section 2. In (a), the white circle represents Earth at departure and the black circle represents Mars at arrival. In (b), the dashed circle illustrates Mars' SOI and the Red Planet is at its centre (not depicted).

3. SYSTEM

The spacecraft is assumed to be a 16-Unit (16U) CubeSat, similar to the MARIO spacecraft designed in [6]. From this, a number of child assumptions can be drawn, regarding:

- **Area**. The largest cross-sectional area of the spacecraft (A) is 0.52 m^2;

- **Mass**. The *wet mass* of the spacecraft (m_{wet}), at departure from Earth's SOI, is 26 kg. In Section 4, mass at the beginning of ballistic capture (m_{BC}) is estimated to be 20.5 kg. This value translates into a mass-to-area ratio $z \approx 40$ kg/m^2;
- **Solar cells**. The cells on the solar panels are Spectrolab's XTJ Prime. With these cells, the spacecraft can be assumed to have a *reflectivity* $C_R = 1.1$;
- **Engine**. The spacecraft engine is Busek's *ion thruster* BIT-3. This engine provides a *thrust magnitude* $T \in [0.66, 1.24]$ mN and *specific impulse* $I_{\text{sp}} \in [1400, 2640]$ s.

Table 2. Assumed spacecraft specifications.

Symbol	Value	Symbol	Range
A	0.52 m^2	T	[0.66, 1.24] mN
m_{wet}	26 kg	I_{sp}	[1400, 2640] s
C_R	1.1	m_{BC}	$\approx$ 20.5 kg

4. BALLISTIC CAPTURE

This section deals with the generation and selection of capture orbits, corresponding to Steps 4 to 6 of the sequence presented in Section 2. The methodology for doing so is explained in Subsections 4.2 and 4.3, and the selected orbits are listed in Subsection 4.4. But before, Subsection 4.1 describes the equations of motion that are used to model the spacecraft environment during ballistic capture.

4.1. Equations of motion

As mentioned in Section 1, ballistic capture is possible because the motion of a spacecraft is influenced by more than one gravitational attractor. So, to design capture at Mars, one needs to model, at least, the *point-mass* gravitational influence of Mars and the Sun. However, [7] provided evidence that ballistic capture at Mars can be made easier by the presence of at least some of the other planets of the Solar System. Furthermore, a high-fidelity model improves the validity of the produced ballistic capture orbits. For those reasons, a Restricted n-Body Problem (RnBP) was simulated, with Mars as the *central body* and the barycentres of the Sun and all planets or satellite systems from Mercury to Neptune as *perturbing bodies*. In addition, Solar Radiation Pressure (SRP) and Mars' Non-Spherical Gravity (NSG) were also included in the model.

The equations of motion can be written, in a non-rotating, Mars-centred reference frame (EME2000) as [2, 8, 9, 10, 11]:

$$\frac{\mathrm{d}^2\vec{r}}{\mathrm{d}t^2} = \vec{f}_{\text{2B}} + \vec{f}_{\text{TB}} + \vec{f}_{\text{SRP}} + \vec{f}_{\text{NSG}} \tag{1}$$

$$\vec{f}_{\text{2B}} \equiv -GM_{\text{M}}\frac{\vec{r}}{r^3} \tag{2}$$

$$\vec{f}_{\text{TB}} \equiv -\sum_{i\in\mathbb{P}} \frac{GM_i}{\|\vec{r}_i - \vec{r}\|^3}\left(q\frac{3+3q+q^2}{1+(1+q)^{\frac{3}{2}}}\vec{r}_i + \vec{r}\right) \tag{3}$$

$$q \equiv \frac{\vec{r}\cdot(\vec{r}-2\vec{r}_i)}{\vec{r}_i\cdot\vec{r}_i} \tag{4}$$

$$\vec{f}_{\text{SRP}} \equiv \frac{Q}{z}\frac{\vec{r}-\vec{r}_S}{\|\vec{r}-\vec{r}_S\|^3}, \quad Q \equiv \frac{L_{\text{S}}C_R}{4\pi c}, \quad z \equiv \frac{m_{\text{BC}}}{A} \tag{5}$$

$$\vec{f}_{\text{NSG}} \equiv -\mathcal{R}\frac{GM_{\text{M}}}{r^2}\left(\Lambda\frac{\vec{r}}{r} - \begin{bmatrix} J \\ K \\ H \end{bmatrix}\right) \tag{6}$$

where: $\vec{f}_{\text{2B}}$ refers to the the 2-body, main force on the right-hand side; $\vec{f}_{\text{TB}}$ refers to the Third-Body (TB) perturbations, written in a formulation that prevents *loss of significance* [12, p. 389]; $\vec{f}_{\text{SRP}}$ refers to the SRP perturbation; $\vec{f}_{\text{NSG}}$ refers to the NSG perturbation, written in a formulation that includes recurrence relations; $\vec{r}$ is the position vector of the spacecraft, with respect to Mars; r is the magnitude of $\vec{r}$; GM_{M} is the gravitational parameter of Mars; $\mathbb{P}$ is a set of $n-2$ indexes, each referencing a perturbing body; $\vec{r}_i$ is the position vector of body i, with respect to Mars; L_{S} is the luminosity of the Sun; c is the speed of light; $\vec{r}_S$ is the position vector of the Sun; $\mathcal{R}$ is the time-dependant matrix that transforms the components of a vector defined in the Mars-fixed frame (IAU-Mars) into components in EME2000; the definitions of Λ, J, K and H can be found in [11].

The infinite series that models $\vec{f}_{\text{NSG}}$ was truncated at *degree* and *order* $n_{\max} = 20$. Finally, numerical experiments showed that if the Martian satellites are not targeted for *flyby*, their presence in the model does not aid ballistic capture and can increase computational time by a factor of 20. This is why the Martian satellites are not included in (1).

4.2. Methodology

To identify ballistic capture orbits, the methodology developed in [2] and [13] was used. In essence, the method requires studying the future and past motion of candidate spacecraft states $\vec{x}(t_0) \equiv \vec{x}_0$, in order to determine which states correspond to ballistic capture orbits.

So, the first step is to define which values of $\vec{x}_0$ shall be tested. Let $\vec{x}_0$ be given by the following *osculating orbital elements*, with respect to a non-rotating, Mars-centred reference frame (RTN@t$_0$ [7]):

$$\begin{aligned}\vec{x}(t_0) &\equiv \{r_p,\ e,\ i,\ \Omega,\ \omega,\ M\}(t_0) \\ &= \{r_{p_0},\ e_0,\ i_0,\ \Omega_0,\ \omega_0,\ 0\} \equiv \vec{x}_0\end{aligned} \tag{7}$$

where: r_p is the *periapsis radius*; e is the *eccentricity*; i is the *inclination*; Ω is the longitude of the *ascending node*, ω is the *argument of periapsis*; M is the *mean anomaly*, which by being equal to zero indicates that the spacecraft is at a periapsis.

To reduce the search space, i_0 and Ω_0 were made equal to $22.5°$ and $0°$, respectively. Past works have shown that higher values of e_0 make capture more likely, so e_0 was made equal to 0.99 [4]. Then, multiple values of ω_0 and r_{p_0} were sampled. For ω_0, a uniform discretisation of $[0, 359]°$ with step $\Delta\omega_0 = 1°$ was used. For r_{p_0}, the interval $R_\text{M} + [250 \text{ km}, 4R_\text{M}]$ was discretised, with step $\Delta r_{p_0} = 25$ km.

Regarding the *arrival times* t_0, the main decision to be made is on the time-span. Since the Earth–Mars synodic period is approximately 780 days, the characteristics of Earth–Mars transfers culminating in ballistic capture should be roughly 780-day periodic. For this reason, a set of t_0 spanning 800 days was investigated. However, one could decide to study any 800-day interval, so a uniform discretisation of $t_{01} + [0, 800]$ days, with step $\Delta t_0 = 50$ days and $t_{01} \equiv$ 08 MAY 2024 12:36:08.639 UTC, was used. t_{01} marks a closest approach of Mars to the Sun.

The second step requires definitions for what constitutes: a) *escape* from Mars; b) one *revolution* of the spacecraft around Mars; c) *impact* with Mars or one of its satellites; d) a maximum *propagation period* Δt_max. The mathematical formulation that was used to define those events can be found in [2] and [13].

With these, one can classify candidate $\vec{x}_0$ based on the future (forwards propagated) and past (backwards propagated) motion of the spacecraft. One says that $\vec{x}_0$ belongs to the *capture set* $\mathcal{C}^6_{-1}$ if: i) the spacecraft completes 6 revolutions around Mars, when propagating forwards, without escaping or impacting with it or with a moon; ii) the spacecraft escapes Mars when propagating backwards. The minimum number of revolutions that the spacecraft should perform around Mars (n) was made equal to 6 to be consistent with previous works on ballistic capture, including [4] and [7].

4.3. Numerical integration

From the previous section, it follows that $N_{\omega_0} \times N_{r_{p_0}} \times N_{t_0} = 360 \times 534 \times 17 = 3{,}268{,}080$ states need to be propagated. That was achieved through numerical integration, using MATLAB's variable-step, variable-order Adams-Bashforth-Moulton scheme `ode113`, with relative and absolute error tolerances set to 10^{-12}.

The number of required propagations is large, but since they are independent from each other, the computational time required for completing them can be decreased with *parallel computing*. This was done using a total of 40 workers.

Finally, all variables and equations of motion were rescaled, to ensure that, throughout the integration, the relative size of the variables does not differ vastly. The length and time units became LU $\equiv R_M$ and TU $\equiv \sqrt{R_M^3/GM_M}$, respectively.

4.4. Orbits for targeting

17 capture sets were generated, each referring to a value t_0 out of the discretisation that was described in Subsection 4.2. Two of these are shown in Figure 2. Each orbit is colour-coded with its value of $S \equiv (t_6 - t_0)/6$, which is *lower* for the more *regular* or repetitive capture orbits [7]. The set of Figure 2a is representative of those with an arrival time $t_0 \in t_{01} + [0, 200] \cup [700, 800]$, when Mars is closer to its perihelion. This type of set contains the most regular orbits, as predicted in [7]. The set of Figure 2b is representative of the remaining arrival times.

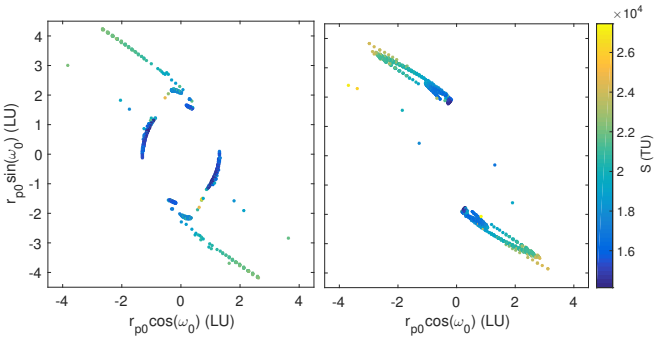

(a) $t_0 = t_{01} + 150$ days. (b) $t_0 = t_{01} + 600$ days.

Fig. 2. Two of the 17 capture sets.

Out of the many capture orbit options offered by each of the 17 sets, only a single orbit of each set was targeted, in Subsection 5.2. This was done to reduce the number of Earth–Mars transfers that had to be designed, but is *not* likely to compromise the generality of the results. To understand why, consider Figure 3. It shows 3 snapshots of the capture trajectories that reach Mars at t_{01}, which the spacecraft will follow if it shuts-off its engine at $t_{01} - \{800,\ 600,\ 400\}$ days, respectively. Two groups of trajectories can be clearly distinguished: one coming from the inside of Mars' orbit, the other from the outside. Since the spacecraft will depart from the Earth, only orbits from the first group were considered, and these are relatively close to each other, especially after $t_{01} - 400$ days.

To select the 17 orbits, preference was given to those with smaller S. The only exception was in the capture set of $t_0 = t_{01} + 450$ days, because its lower-S orbits had already been revolving around Mars for 400 days prior to t_0. The algorithm did not notice this early arrival because the orbit keeps reversing its sense of motion before t_0, so no revolutions were counted (see [2] for additional details).

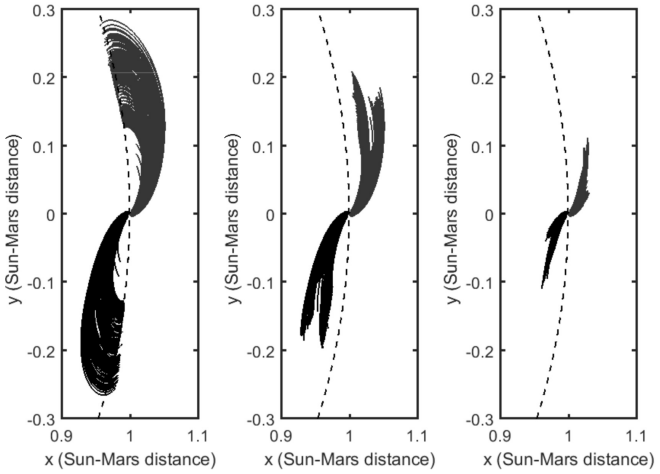

(a) − 800 days. (b) − 600 days. (c) − 400 days.

Fig. 3. Snapshots of capture trajectories which reach at Mars at $t = t_{01}$. The reference frame is the RPF, as defined in [14]. The dashed line is a circle of unitary radius.

5. LOW-THRUST TARGETING

This section deals with the design of the transfers to the ballistic capture orbits that were selected in Section 4, corresponding to Steps 1 to 3 of the sequence presented in Section 2. The methodology for doing so is explained in Subsections 5.2 and 5.3. But before, Subsection 5.1 describes the equations of motion that are used to model the spacecraft environment during the powered transfer. In addition, Subsection 5.4 presents some transfers that simply rendezvous with Mars, *without* ballistic capture, which serve as basis for comparison, in Section 6.

5.1. Equations of motion

Before deciding on the model, a few transfers to ballistic capture were designed, either with the complete Heliocentric dynamics ($\vec{f}_{2\mathrm{B}}$, $\vec{f}_{\mathrm{TB}}$ and $\vec{f}_{\mathrm{SRP}}$) or simply the Sun's gravitational attraction ($\vec{f}_{2\mathrm{B}}$). The transfers showed only negligible differences, so the inclusion of the extra force fields was deemed unnecessary for this early phase of trajectory design. It makes sense, because during the ballistic capture stage, the perturbations are *actively being exploited*, to get the spacecraft to perform the required number of revolutions around Mars. On the other hand, during the heliocentric transfer, the spacecraft has its engine to *manoeuvre*, so most of the dynamics are simply the background against which the transfer takes place.

With state vector $\vec{x} \equiv \{r,\, \theta,\, \phi,\, v_r,\, v_\theta,\, v_\phi,\, m\}$ and control $\vec{u} \equiv \{T,\, \alpha,\, \beta\}$, the equations of motion are [15, 16, 17]:

$$\frac{\mathrm{d}\vec{x}}{\mathrm{d}t} = \begin{bmatrix} v_r \\ v_\theta/(r\cos\phi) \\ v_\phi/r \\ \begin{bmatrix} -GM_{\mathrm{S}}/r^2 \\ 0 \\ 0 \end{bmatrix} + \mathcal{S} \begin{bmatrix} v_r \\ v_\theta \\ v_\phi \end{bmatrix} + \vec{f}_T \\ -T/(I_{\mathrm{sp}}\, g_0) \end{bmatrix} \tag{8}$$

$$\mathcal{S} \equiv \begin{bmatrix} 0 & \dot{\theta}\cos\phi & \dot{\phi} \\ -\dot{\theta}\cos\phi & 0 & \dot{\theta}\sin\phi \\ -\dot{\phi} & -\dot{\theta}\sin\phi & 0 \end{bmatrix} \tag{9}$$

$$\vec{f}_T \equiv \frac{T}{m} \begin{bmatrix} \sin\alpha\cos\beta \\ \cos\alpha\cos\beta \\ \sin\beta \end{bmatrix} \tag{10}$$

where: *spherical coordinates* were used, to ensure that the state variables change slowly, thereby reducing the number of points required for their discretisation in time; GM_{S} is the gravitational parameter of the Sun; α and β are the azimuth and elevation of the *thrust vector*, with respect to the direction of v_θ; g_0 is the standard gravitational acceleration; m is the mass of the spacecraft.

5.2. Methodology

The transfers to ballistic capture were stated as an *optimal control* problem. Then, this problem was transcribed into a Nonlinear Programming (NLP) problem, by means of a *collocation* method.

The optimal control problem contains three parts. The first is a *mathematical model*, given by Equation (9). The second part is a task description, stated by the following *boundary conditions* and *path constraints*:

$$\begin{array}{ll} t_d = t_0 - \Delta t_{\mathrm{TOF}} & t_f \le t_\infty \\ r(t_d) = r_{\mathrm{E}}(t_d) + R_{\mathrm{SOI_E}} & r(t_f) = r_{\mathrm{C}}(t_f) \\ \theta(t_d) = 0 & \theta(t_f) = \theta_{\mathrm{C}}(t_f) + 2\pi\Delta n \\ \phi(t_d) = 0 & \phi(t_f) = \phi_{\mathrm{C}}(t_f) \\ v_r(t_d) = v_{r\mathrm{E}}(t_d) & v_r(t_f) = v_{r\mathrm{C}}(t_f) \\ v_\theta(t_d) = v_{\theta\mathrm{E}}(t_d) & v_\theta(t_f) = v_{\theta\mathrm{C}}(t_f) \\ v_\phi(t_d) = 0 & v_\phi(t_f) = v_{\phi\mathrm{C}}(t_f) \\ m(t_d) = m_{\mathrm{wet}} & m(t_f) \text{ free} \\ \\ \alpha(t) \le \pi & T(t) \le 1.24 \text{ mN} \\ \alpha(t) \ge -\pi & r(t) \ge 0.1\, r_d \\ \beta(t) \le \pi/2 & m(t) \le m_{\mathrm{wet}} \\ \beta(t) \ge -\pi/2 & m(t) \ge 1 \text{ kg} \end{array} \tag{11}$$

where: the conditions of Earth are marked with the index E; the capture conditions are marked with the index C and are

obtained through backwards propagation of the states $\vec{x}_0$ in $\mathcal{C}^6_{-1}$; t_0 is a *parameter* of the optimisation, to be picked from the alternatives defined in Subsection 4.2; Δt_{TOF} is the total Time of Flight (TOF) and is also a parameter, to be picked from $[1200, 2200]$ days, with a 50-day step; Δn controls the number of *extra* revolutions that the spacecraft performs, with respect to the ballistic capture point, and is again a parameter, to be picked from $\{0, 1, 2, 3\}$; t_f has been restricted to values below the time t_∞ at which the spacecraft first enters the SOI of Mars; the bounds on r and m were placed to help with the convergence of the numerical method.

The third and final part is a *performance index* (J), which was defined as $-m_f$, to make it a *fuel*-optimal problem. This choice of performance index guarantees that the optimal solutions have either $T = 0$ or $T = T_{\max}$ [18]. That, in turn, means that one can make $I_{\text{sp}} = I_{\text{sp}_{\max}}$, in Equation (9), without any loss of generality.

Taking into account all the parameters, the number of optimal control problems to be solved is $N_{t_0} \times N_{\Delta t_{\text{TOF}}} \times N_{\Delta n} = 17 \times 21 \times 4 = 1428$. To transcribe these problems with direct collocation, the time interval $[t_d, t_f]$ was discretised into nodes, $\vec{u}$ approximated by a linear function at each subinterval and $\vec{x}$ by defect constraints $\vec{\zeta}$: [18]

$$\begin{gathered} t_d = t_1 < t_2 < \cdots < t_{N-1} < t_N = t_f\,, \\ \vec{u}(t_k) \equiv \vec{u}_k\,, \quad \vec{x}(t_k) \equiv \vec{x}_k \\ \\ t_k \leq t \leq t_{k+1}\,, \\ \vec{u}(t) = \vec{u}_k + \frac{t - t_k}{t_{k+1} - t_k}\,(\vec{u}_{k+1} - \vec{u}_k) \\ \vec{\zeta}_k(\vec{x}_k, \vec{x}_{k+1}, \vec{u}_k, \vec{u}_{k+1}, t_k, t_{k+1}) = \vec{0} \end{gathered} \tag{12}$$

where: the discretisation is *uniform* and N was chosen equal to 400; the *Hermite-Simpson* method was used to construct the defect constraints from Equation (9). [19, 18]

The NLP variables are then $\vec{y} \equiv \{\vec{x}_d, \vec{u}_d, \vec{x}_2, \vec{u}_2, \ldots, \vec{x}_f, \vec{u}_f, t_f\}$. Boundary conditions and objective function are already functions of $\vec{y}$, but not the path constraints, which are originally functions of variables continuous over time $t \in [t_d, t_f]$. For that reason, they were enforced at each node, with each path constraint being represented by 400 discrete constraints. [18]

5.3. Numerical method

The NLP problem was solved with an Interior Point Method (IPM), implemented by the IPOPT solver, which is publicly available in its COIN-OR page. It was set to use a *quasi-Newton* Nonlinear Algebraic Equation (NAE) solver and terminate successfully when: the *optimality error*, defined in [20], is lower than 10^{-6}; the absolute value of the constraint *residual* is less than 10^{-12}. The maximum number of iterations was set at 5000.

Two additional comments are in order: i) the Jacobian of the constraints (defect, boundary and path) was derived *analytically* and supplied to IPOPT, to speed up the computations; ii) the capture conditions $\vec{x}_C(t)$, which are terminal conditions in Equation (11), were provided to IPOPT in the form of a *cubic spline*, created with MATLAB function `spline`. The spline interpolates one of the 17 capture trajectories, backwards propagated from $\vec{x}_0$, using the points selected by `ode113`.

Finally, just like in Section 4.3, the variables and equations of motion were rescaled. The length, time and mass units became LU $\equiv r_{1\text{AU}}$, TU $\equiv \sqrt{r^3_{1\text{AU}}/GM_{\text{S}}}$ and MU $\equiv m_{\text{wet}}$, respectively.

5.4. Rendezvous with Mars

Before actually designing the trajectories that culminate in ballistic capture, it is convenient to first produce some transfers that are more standard, for comparison purposes. For that reason, some simple rendezvous with Mars were generated, with terminal conditions:

$$\begin{array}{ll} r(t_f) = r_{\text{M}}(t_f) - R_{\text{SOIM}} & v_r(t_f) = v_{r\text{M}}(t_f) \\ \theta(t_f) = \theta_{\text{M}}(t_f) + 2\pi\Delta n & v_\theta(t_f) = v_{\theta\text{M}}(t_f) \\ \phi(t_f) = \phi_{\text{M}}(t_f) & v_\phi(t_f) = v_{\phi\text{M}}(t_f) \\ t_f = t_{\infty\text{rv}} & m(t_f) \text{ free} \end{array} \tag{13}$$

where: the conditions of Mars are marked with the index M; for consistency with the ballistic capture orbits, t_f was fixed at $t_{\infty\text{rv}}$, defined as the time at which the spacecraft would cross the SOI of Mars, provided that at t_0 it has to be at the periapsis. Assuming that the rendezvous would lead to a parabolic Keplerian orbit with $r_p \approx 4621$ km, this time was estimated to be $t_0 - 12$ days.

The rest of the problem statement was kept identical to the one of Subsection 5.2. Figure 4a shows the required mass of propellant $\Delta m \equiv m(t_f) - m(t_d)$, for each pair of arrival date and TOF (t_0, Δt_{TOF}). Most of the plot shows a similar Δm. The innermost contour line corresponds to $\Delta m = 5.1$ kg and delimits a large area where the required mass of propellant varies by no more than 0.2 kg. The white region marks the *infeasible* pairs $\{t_0, \Delta t_{\text{TOF}}\}$, with the boundary corresponding to the *time*-optimal transfers.

To get some additional insight on why Figure 4a looks the way it does, consider Figure 4b, which shows $\Delta\theta \equiv \theta(t_f) - \theta(t_d)$. In it, one can see two discontinuities in required number of revolutions, marked by the two sets of very close contour lines (MATLAB's `contourf` does not recognise discontinuities). These correspond to the Δm peaks in Figure 4a, which makes sense, because at these discontinuities, the spacecraft must either speed up to reach the target with one less revolution or slow down to reach it with one more. Also, notice that the feasibility boundary to the right of $t_0 = t_{01} + 150$ days is aligned with one of the discontinuities.

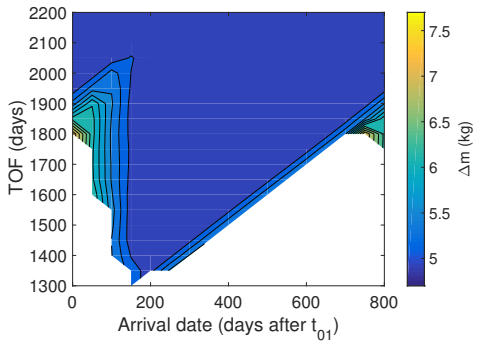

(a) Δm.

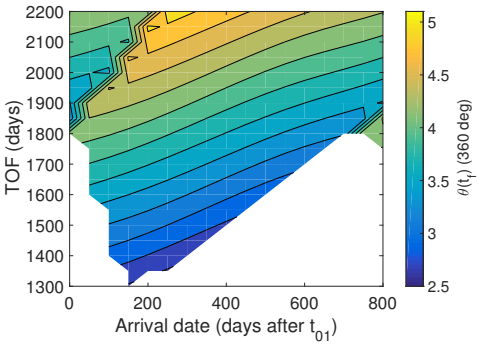

(b) $\Delta\theta$.

Fig. 4. Results of the rendezvous with Mars, as functions of $\{t_0,\, \Delta t_{\text{TOF}}\}$. The contour lines are drawn: a) every 0.2 kg, from 5.1 to 7.1 kg; b) every $0.2 \cdot 360°$, from 2.9 to $4.9 \cdot 360°$.

6. RESULTS

Figure 5 reports the results of the transfers to ballistic capture. Figure 5a shows the required mass of propellant Δm, for each pair $\{t_0,\, \Delta t_{\text{TOF}}\}$. Just like for the rendezvous, in Subsection 5.4, most of the plot shows a similar Δm. In fact, the similarity of Figures 4a and 5a is clear. The innermost contour line now corresponds to $\Delta m \approx 4.9$ kg, which differs only -0.2 kg from than one of Figure 4a. This makes sense because the patching point with ballistic capture is close to Mars' orbit (see Figure 3), so the targets for rendezvous or capture are close-by and moving at similar velocities. With this, two important remarks can be made: i) in a low-thrust transfer culminating in ballistic capture, the revolutions that the spacecraft is guaranteed to perform around Mars are *cost-free*, with respect to the rendezvous' flyby; ii) a CubeSat may have the propulsion capabilities to conduct a stand-alone mission to Mars which culminates in ballistic capture, requiring only about 20% of its initial mass to be propellant.

The fuel-optimal transfer with the smallest TOF lasts for 1300 days and arrives at $t_{01} + 150$ days (keep in mind that the discretisation used in this grid search has a 50-day step). This TOF of about 3.5 years is somewhat long, considering

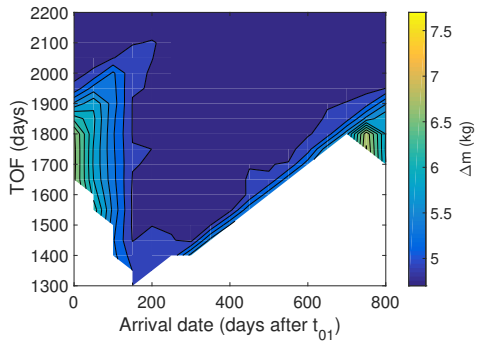

(a) Δm.

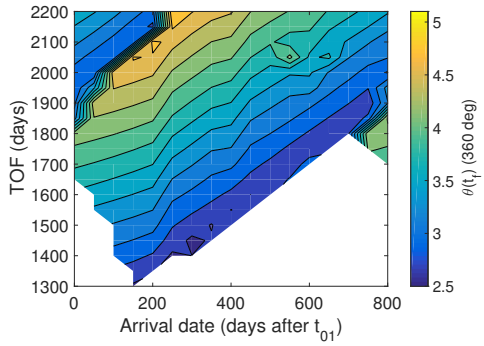

(b) $\Delta\theta$.

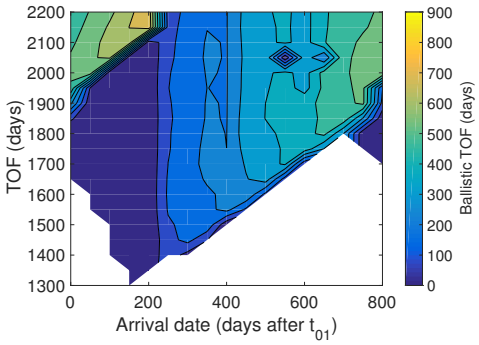

(c) Δt_{BTOF}.

Fig. 5. Results of the transfer to capture, as functions of $\{t_0,\, \Delta t_{\text{TOF}}\}$. The contour lines are drawn: a) every 0.2 kg, from 4.9 to 6.9 kg; b) every $0.2 \cdot 360°$, from 2.7 to $4.7 \cdot 360°$; c) every 75 days, from 75 to 675 days.

that the travel to Mars is known to expose the spacecraft to radiation, which can damage the COTS components typically used in CubeSats. Finally, Figure 5c shows the Ballistic TOF (BTOF) $\Delta t_{\text{BTOF}} \equiv t_0 - t_f$, that is, the time between the spacecraft permanently shutting off its engine and reaching the first closest approach to Mars. When Δt_{BTOF} is lowest, it means that the transfer is almost a rendezvous with the SOI of Mars.

7. CONCLUSIONS

The present work aimed to determine the characteristics of Earth–Mars transfers that combine ballistic capture with low-thrust propulsion. A technique was developed to produce such transfers and was applied to a 16U CubeSat mission. The results support the conclusion that such a CubeSat may be capable of conducting a stand-alone mission to Mars.

Still, some direct follow-ups are in order, including: a) investigating the radiation dose accumulated by the spacecraft during the 1300-day transfer to ballistic capture and inferring the likelihood of it surviving such a trip; b) including the Earth-escape phase of the mission in the trajectory design process, by trading-off escape strategies. If the spacecraft leaves the SOI of Earth with some excess velocity, Mars can be reached faster (and cheaper).

8. REFERENCES

[1] E. Belbruno, *Fly me to the moon: An insider's guide to the new science of space travel*, Princeton University Press, Woodstock, United Kingdom, 2013.

[2] Z.-F. Luo, F. Topputo, F. Bernelli-Zazzera, and G. J. Tang, "Constructing ballistic capture orbits in the real Solar System model," *Celestial Mechanics and Dynamical Astronomy*, vol. 120, no. 4, pp. 433–450, 2014.

[3] Sara Spangelo and Benjamin Longmier, "Optimization of CubeSat System-Level Design and Propulsion Systems for Earth-Escape Missions," *Journal of Spacecraft and Rockets*, vol. 52, no. 4, pp. 1009–1020, 2015.

[4] F. Topputo and E. Belbruno, "Earth–Mars transfers with ballistic capture," *Celestial Mechanics and Dynamical Astronomy*, vol. 121, no. 4, pp. 329–346, 2015.

[5] Pablo Moral, Simone Centuori, and Manuel Sanjurjo-Rivo, "Ballistic capture and transfer opportunities for a mission to Mars," *68th International Astronautical Congress*, 2017.

[6] Á. S. Casado, "Preliminary Systems Design of a Stand-Alone Interplanetary CubeSat to Mars," M.S. thesis, Universidad Carlos III de Madrid, Politecnico di Milano, 2017.

[7] Z.-F. Luo and F. Topputo, "Analysis of ballistic capture in Sunâ–planet models," *Advances in Space Research*, vol. 56, no. 6, pp. 1030–1041, 2015.

[8] Roberto Barrio and Sergio Serrano, "Performance of perturbation methods on orbit prediction," *Mathematical and Computer Modelling*, vol. 48, pp. 594–600, 2008.

[9] Ryan P Russell, "Survey of Spacecraft Trajectory Design in Strongly Perturbed Environments," *Journal of Guidance, Control, and Dynamics*, vol. 35, no. 3, pp. 705–720, 2012.

[10] Daniel P. Lubey and Daniel J. Scheeres, "Identifying and Estimating Mismodeled Dynamics via Optimal Control Policies and Distance Metrics," *Journal of Guidance, Control, and Dynamics*, vol. 37, no. 5, pp. 1512–1523, 2014.

[11] Robert G. Gottlieb, "Fast Gravity, Gravity Partials, Normalized Gravity, Gravity Gradient Torque and Magnetic Field: Derivation, Code and Data," Tech. Rep. 188243, Lyndon B. Johnson Space Center, 1993.

[12] R. H. Battin, *Introduction to the Mathematics and Methods of Astrodynamics*, American Institute of Aeronautics and Astronautics, Reston, United States of America, 2000.

[13] Z.-F. Luo and F. Topputo, "Capability of satellite-aided ballistic capture," *Communications in Nonlinear Science and Numerical Simulation*, vol. 48, pp. 211–223, 2017.

[14] Diogene A. Dei Tos and Francesco Topputo, "Trajectory refinement of three-body orbits in the real solar system model," *Advances in Space Research*, vol. 59, no. 8, pp. 2117–2132, 2017.

[15] Christopher Louis Ranieri, *Indirect Optimization of Interplanetary Trajectories Including Spiral Dynamics*, Ph.D. thesis, University of Texas at Austin, 2007.

[16] John T. Betts and Sven O. Erb, "Optimal Low Thrust Trajectories to the Moon," *SIAM Journal on Applied Dynamical Systems*, vol. 2, no. 2, pp. 144–170, 2003.

[17] Chen Zhang, F. Topputo, F. Bernelli-Zazzera, and Y. Zhao, "Low-Thrust Minimum-Fuel Optimization in the Circular Restricted Three-Body Problem," *Journal of Guidance, Control, and Dynamics*, vol. 38, no. 8, pp. 1501–1509, 2015.

[18] F. Topputo and C. Zhang, "Survey of direct transcription for low-thrust space trajectory optimization with applications," *Abstract and Applied Analysis*, vol. 2014, 2014.

[19] J. T. Betts, "Survey of Numerical Methods for Trajectory Optimization," *Journal of Guidance, Control, and Dynamics*, vol. 21, no. 2, pp. 193–207, 1998.

[20] Andreas Wächter and Lorenz T Biegler, "On the Implementation of an Interior Point Filter Line Search Algorithm for Large-Scale Nonlinear Programming," *Mathematical Programming*, vol. 106, no. 1, pp. 25–57, 2005.